

PAPER • OPEN ACCESS

Multi-slice electron ptychographic tomography for three-dimensional phase-contrast microscopy beyond the depth of focus limits

To cite this article: Andrey Romanov *et al* 2025 *J. Phys. Mater.* **8** 015005

View the [article online](#) for updates and enhancements.

You may also like

- [From wide to ultrawide-bandgap semiconductors for high power and high frequency electronic devices](#)
Kelly Woo, Zhengliang Bian, Malisha Noshin et al.
- [2024 roadmap on 2D topological insulators](#)
Bent Weber, Michael S Fuhrer, Xian-Lei Sheng et al.
- [Soft matter roadmap](#)
Jean-Louis Barrat, Emanuela Del Gado, Stefan U Egelhaaf et al.

The advertisement features a blue background with circular ECS logos at the top and bottom. In the center, there's a photo of a smiling woman in a brown blazer. To her left, text reads: "UNITED THROUGH SCIENCE & TECHNOLOGY", "ECS The Electrochemical Society Advancing solid state & electrochemical science & technology", "248th ECS Meeting Chicago, IL", "October 12-16, 2025 Hilton Chicago". To her right, large text says "Science + Technology + YOU!". At the bottom, a button says "REGISTER NOW". On the right side, text says "Register by September 22 to save \$\$".

Journal of Physics: Materials

**OPEN ACCESS****RECEIVED**
23 August 2024**REVISED**
22 November 2024**ACCEPTED FOR PUBLICATION**
5 December 2024**PUBLISHED**
16 December 2024

Original Content from
this work may be used
under the terms of the
[Creative Commons
Attribution 4.0 licence](#).

Any further distribution
of this work must
maintain attribution to
the author(s) and the title
of the work, journal
citation and DOI.

**PAPER**

Multi-slice electron ptychographic tomography for three-dimensional phase-contrast microscopy beyond the depth of focus limits

Andrey Romanov¹ , Min Gee Cho^{2,3} , Mary Cooper Scott^{2,3,4} and Philipp Pelz^{1,*} ¹ Institute of Micro- and Nanostructure Research (IMN) & Center for Nanoanalysis and Electron Microscopy (CENEM), Friedrich Alexander-Universität Erlangen-Nürnberg, IZNF, 91058 Erlangen, Germany² National Center for Electron Microscopy, Molecular Foundry, Lawrence Berkeley National Laboratory, Berkeley, CA 94720, United States of America³ Department of Materials Science and Engineering, University of California Berkeley, Berkeley, CA 94720, United States of America⁴ Materials Sciences Division, Lawrence Berkeley National Laboratory, Berkeley, CA 94720, United States of America

* Author to whom any correspondence should be addressed.

E-mail: philipp.pelz@fau.de**Keywords:** ptychography, electron microscopy, computational imaging, tomographySupplementary material for this article is available [online](#)**Abstract**

Electron ptychography is a powerful computational method for atomic-resolution imaging with high contrast for weakly and strongly scattering elements. Modern algorithms coupled with fast and efficient detectors allow imaging specimens with tens of nanometers thicknesses with sub-0.5 Ångstrom lateral resolution. However, the axial resolution in these approaches is currently limited to a few nanometers, limiting their ability to solve novel atomic structures *ab initio*. Here, we experimentally demonstrate multi-slice ptychographic electron tomography, which allows atomic resolution three-dimensional phase-contrast imaging in a volume surpassing the depth of field limits. We reconstruct tilt-series 4D-STEM measurements of a Co₃O₄ nanocube, yielding 2 Å axial and 0.7 Å transverse resolution in a reconstructed volume of (18.2 nm)³. Our results demonstrate a 13.5-fold improvement in axial resolution compared to multi-slice ptychography while retaining the atomic lateral resolution and the capability to image volumes beyond the depth of field limit. Multi-slice ptychographic electron tomography significantly expands the volume of materials accessible using high-resolution electron microscopy. We discuss further experimental and algorithmic improvements necessary to also resolve single weakly scattering atoms in 3D.

1. Introduction

Aberration-corrected scanning transmission electron microscopy (STEM) is a highly potent technique for visualizing materials at the atomic level and analyzing their chemical makeup. Advances in equipment, insights into the interactions between electrons and matter, and automation and data analysis enhancements have propelled its prominence for materials characterization. Lately, the application of computational imaging approaches that leverage 2D position- and 2D momentum-resolved measurements (4D-STEM) has emerged as a formidable method, enabling the imaging of heavy and light elements, pinpointing atomic positions with picometer-level accuracy, and charting out phase, orientation, and strain across extensive areas. With the latest generation of ultrafast direct electron detectors (DEDs), new capabilities and methods that were previously inaccessible are unlocked. Fast DEDs' high detective quantum efficiency allows imaging of beam-sensitive materials at unprecedented resolution and precision. Computational imaging methods like integrated center of mass imaging (iCOM) [1], optimum bright-field (OBF) imaging [2], and electron ptychography [3] utilize 4D-STEM datasets to produce high-contrast, high-resolution images of beam-sensitive materials like metal-organic frameworks and zeolites [4, 5], Li-ion battery materials [6], polymers and perovskite materials [7]. A new frontier of electron microscopy is the recovery of

three-dimensional information from 4D-STEM datasets. The motivation for extracting three-dimensional atomic resolution information from materials is given by our ability to tailor materials properties through engineering e.g. strain, defects, interfaces, and polarization at the atomic scale and induce novel material functionalities. Three-dimensional imaging methods can be classified into depth sectioning methods, which recover 3D information without tilting the specimen, and tomographic methods, which recover 3D information from tilt-series data. Both branches can be subdivided into incoherent methods, which do not model wave propagation within the sample, and coherent methods, which provide phase contrast and often allow modeling and recovering aberrations and other nuisance parameters. Coherent depth sectioning in the STEM was first demonstrated on weakly scattering nanomaterials from a single 4D-STEM dataset using multi-slice electron ptychography (MSP) [8]. More recent work employing an advanced MSP reconstruction algorithm allowed the solution of multiple scattering in thick crystalline slabs and reaching the physical resolution limits in the transverse direction [9]. Additionally, MSP can surpass the axial resolution limit set by the numerical aperture of the electron optics at high electron fluences. So far, an axial resolution of 2.74 nm has been demonstrated using this method [10]. MSP has since been applied to a wealth of materials, resulting in high-resolution imaging of zeolites [11], three-dimensional imaging of dislocation cores in SrTiO₃ [12], and computational crystal mistilt correction [13]. This quick adaptation of MSP to study different materials systems demonstrates the usefulness of 3D phase-contrast imaging based on 4D-STEM. However, sub-nanometer resolution using this technique can only be expected with extremely high fluence and the most advanced electron optics [14].

Incoherent depth sectioning can be performed using the high-angle annular dark-field (HAADF) signal. Focal-series HAADF-STEM can be used to obtain three-dimensional depth sections with several nanometer axial resolution [15–22]. Further depth sectioning approaches include center-of-mass based depth sectioning [23], S-matrix virtual depth sectioning from 4D-STEM focal series [24, 25], and virtual sectioning from multi-segment detectors [26–28].

A solution to the problem of limited axial resolution is the collection of tilt-series measurements and subsequent tomographic reconstruction. This approach yields 3D atomic resolution volumes but comes with the additional complexity of aligning atomic-resolution high-dimensional datasets. Ptychographic electron tomography was first realized at the nanoscale [29], demonstrating improved contrast for imaging hybrid materials. Atomic resolution single-slice ptychographic tomography (SSPT) was recently demonstrated on a 2D material [30] and on a complex double-wall carbon nanotube filled with a Zr₁₁Te₅₀ structure [31].

These works used the projection approximation to reconstruct 2D projection images of the sample, from which the 3D atomic structure was either directly determined by peak fitting [30], or a 3D volume was reconstructed from which an atomic model was determined [31]. The projection approximation limits the applicability of this approach to a few nanometer-thick materials.

ADF-STEM-based atomic resolution tomography [32] was developed to solve the atomic structure of metallic nanoparticles and 2D materials [33]. It is also limited by the projection approximation.

The depth resolution of focal-series HAADF-STEM can be increased if a combined focal-tilt series is recorded and the three-dimensional contrast transfer function is iteratively deconvolved. This approach has been demonstrated at nanometer-scale resolution both using Fourier-space deconvolution [34, 35] and real-space deconvolution [36–38]. Atomic resolution imaging should also be achievable [39].

Many coherent approaches for three-dimensional imaging using scanning diffraction measurements originate in x-ray or visible light microscopy, where they are seeing widespread application. The foundation for later tomographic algorithms extending beyond the depth of field limit was laid with the realization of MSP [40] at visible wavelengths. Later, this algorithm was applied also in the hard x-ray regime [41, 42]. Still, the application has been limited to proof-of-principle demonstrations, mainly because the depth of field of x-ray optics is quite large, and modeling propagation or multiple scattering within the sample is often unnecessary. The first demonstration of a sequential approach to ptychographic tomography showed a 3D reconstruction of bone at 150 nm resolution using hard x-rays and zone-plate optics [43]. This approach is now prevalent at many x-ray beamlines worldwide, offering improved resolution and sensitivity compared to other phase-contrast imaging methods. The sequential algorithm can be improved by reconstructing the volume directly from the diffraction measurements in a joint reconstruction using the single-slice approximation [44–47]. The next step in model complexity is to solve a multi-slice ptychography problem at every tilt angle and then use this information in a subsequent tomography reconstruction. This sequential approach to multi-slice ptychographic tomography (MSPT) has been realized in proof-of-principle experiments at visible [48] and x-ray [49] wavelengths. The multi-slice ptychographic and tomographic reconstructions can also be combined in a joint MSPT reconstruction algorithm that couples all diffraction measurements directly to the reconstructed volume without intermediate results [50–54]. This approach requires good initial guesses of all nuisance parameters and has not been realized yet experimentally. Another interesting experimental development is precession MSP [55], where the sample is tilted to a few small

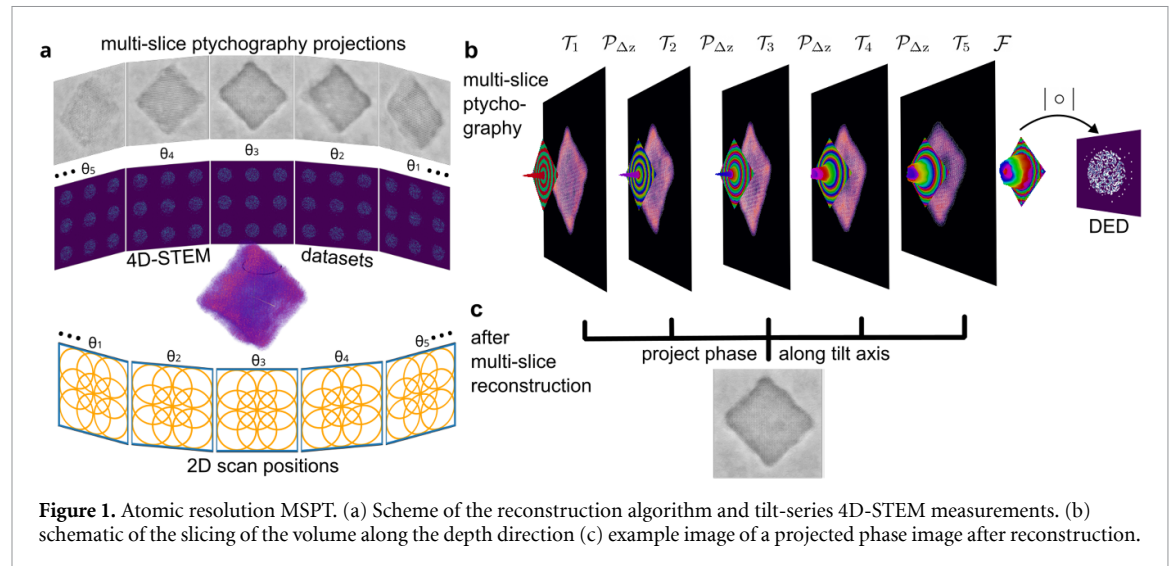


Figure 1. Atomic resolution MSPT. (a) Scheme of the reconstruction algorithm and tilt-series 4D-STEM measurements. (b) schematic of the slicing of the volume along the depth direction (c) example image of a projected phase image after reconstruction.

angles, and a joint 3D reconstruction is performed from these angles with increased axial resolution. This approach might be desirable in STEM since precession is achieved routinely with electron optics by tilting the electron beam instead of the sample.

Ptychographic electron tomography using 4D-STEM was first proposed at atomic resolution [56] using multislice simulations. Due to the success of ADF-STEM-based atomic resolution tomography, Chang *et al* proposed a sequential method for SSPT [57], showing improved contrast for weakly scattering elements. Joint multi-slice electron ptychographic tomography has been considered again recently, this time using the entire tilt range available in the TEM and compared with single-slice reconstruction [58] and improved reconstruction compared to a sequential approach demonstrated in simulation. Another approach to 3D phase-contrast imaging with ptychography used the single-particle assumption to image the volume of a virus particle from many identical copies [59].

Here, we advance atomic-scale three-dimensional phase contrast imaging in the STEM by experimentally demonstrating a sequential MSPT approach in a volume breaking the depth of field limit by a factor of 3.7 and at a resolution that allows us to distinguish single Cobalt atoms in a Co_3O_4 nanocube.

2. Results

2.1. Experiment

Figure 1 shows the overall scheme of the sequential approach for MSPT. At each tilt angle $\theta_{\{1\dots n\}}$, a 4D-STEM scan is taken with overlapping probes as indicated in figure 1(a) bottom panel, resulting in one ptychographic 4D-STEM dataset per tilt angle. In figure 1(a) middle panel, each of these 4D-STEM datasets is then reconstructed using an MSP algorithm, and the phase of all reconstructed slices is summed along the beam direction. Examples of the resulting projected phase images are shown in figure 1(a) top panel.

The principle of the MSP forward model is shown in figure 1(b). In figure 1(b), a convergent illumination wave function is incident on the sample volume, represented by several complex-valued slices that represent the 3D transmission function of the sample. The wave function is first transmitted at each slice and then propagated in free space using Fresnel propagation. As a last step, the wave function is propagated to the detector plane in the far field of the sample, and its intensity is recorded on a DED. After reconstruction of the phase projections with MSP, they are denoised using the BM3D algorithm [60] and used as input for a tomographic reconstruction algorithm.

Synthesis conditions of the Co_3O_4 nanocube sample are described in supplementary section 1. Such Co_3O_4 nanocubes have been used as building blocks for a new type of strain-engineered core–shell nanoparticles [61]. We recorded 36 4D-STEM datasets [62] with full diffraction patterns over 800×800 probe positions at each tilt angle. The experimental details are described in supplementary section 2 and the experimental and reconstruction parameters in supplementary sections 4 and 5. The experimental parameters amounted to an accumulated fluence of $4.6 \times 10^4 \text{ e} \text{\AA}^{-2}$ per projection and $1.6 \times 10^6 \text{ e} \text{\AA}^{-2}$ for the whole tilt series. For each 4D-STEM dataset, we perform an MSP reconstruction [13] using the parameters in supplementary table 2. Since the Co_3O_4 cube has a side length of about 13 nm, and the images a field of view of 18.2 nm, we reconstruct a total of five slices with 3 nm thickness along the depth of the cube, corresponding to a slight oversampling of the depth of field along the axial direction, given that the depth of

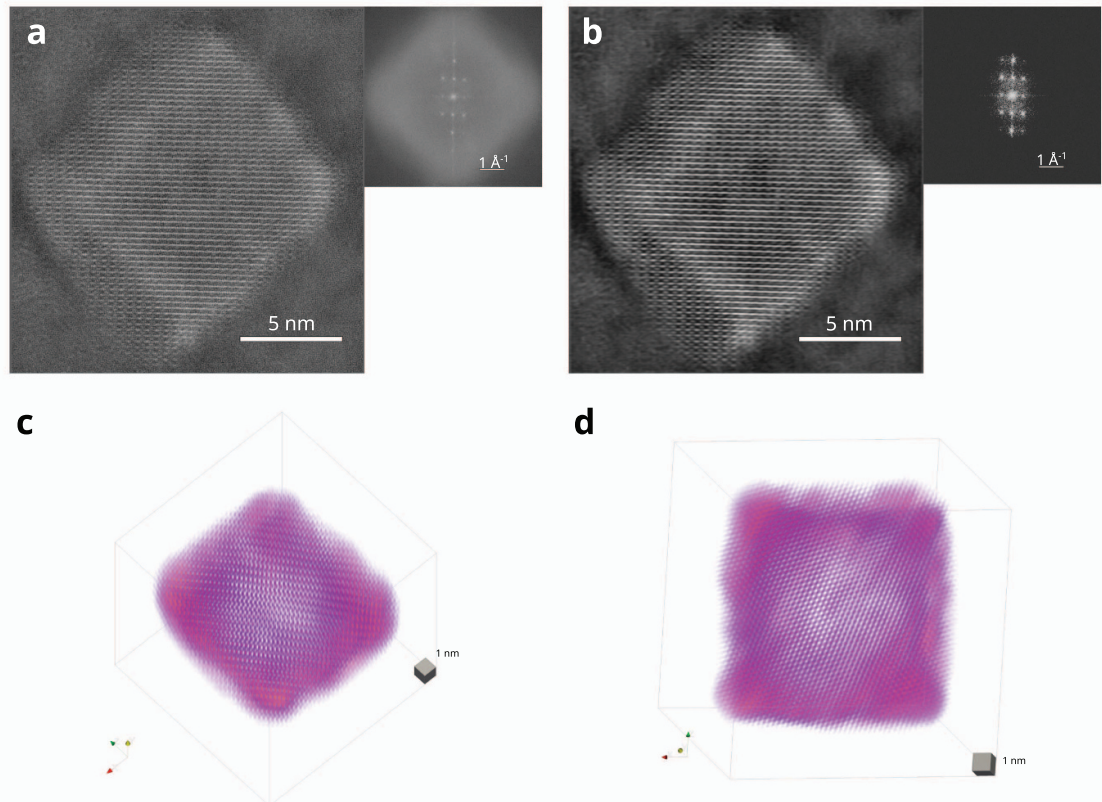


Figure 2. Exemplary ptychographic reconstruction (a) before and (b) after denoising. (c) Reconstructed volume, oriented along the $[11\bar{2}]$ direction. (d) reconstructed volume viewed along the $[228]$ direction.

focus in our experiment was 5 nm. Exemplary reconstructed summed slices of the phase-contrast images are shown in the top panel of figure 1(a), and examples of experimental diffraction patterns for each angle below the reconstructed phase images. Phase-contrast images from the entire dataset are shown in supplementary figure 1.

2.2. Tomography reconstruction

After the MSP reconstruction, we apply denoising using BM3D denoising as performed in ADF-STEM tomography [63], followed by a Fourier-sparsity constraint to de-emphasize the contrast contribution from the high spatial frequency noise. A Fourier-sparsity constraint is justified since we are imaging a single-grain nanoparticle. A Fourier sparsity constraint would be less suitable for more complex and disordered materials. The results of this denoising process are shown by example in figure 2(a) with a reconstructed phase projection and figure 2(b) with the resulting denoised image. The corresponding power spectra are shown in the insets. From the initially-aligned tilt series, we then perform a 3D reconstruction using joint reconstruction and rigid alignment as in [31], implemented with the automatic gradient calculation of the pytorch package [64] using the projections obtained from MSP shown in figure 1(a).

Accurate translational and angular alignment is crucial for high-resolution, large-volume tomography reconstruction close to the Nyquist limit. To refine the tilt series alignment, we devised a two-step optimization algorithm for 3D reconstruction from downsampled projection images, shown in figure 3. As a forward model, we used an affine transformation (rotation and translation) of the reconstructed volume and then projection onto the specified axis. Comparing the obtained projections with the reference ones using the pixel-wise mean squared error (MSE) loss function, we calculate the loss value for minimization through backpropagation and gradient descent with the Adam algorithm. Within the inner loop, as a first step, we reconstruct the volume with a fixed alignment, and in the outer loop, we refine the alignment with the fixed resulting volume. We executed this algorithm first with a 10% resolution of the original ptychographic images for translation optimization and then with 20% resolution of the original for rotation optimization. Furthermore, we applied a 40% intensity threshold to the original projections before down-scaling to mitigate noise and accentuate the contours of the nanocube.

Further, we utilized the resulting down-scaled reconstructed volume to build a full-scale mask volume (see supplementary figure 3) by binarization after a certain value and following blurring, which quite

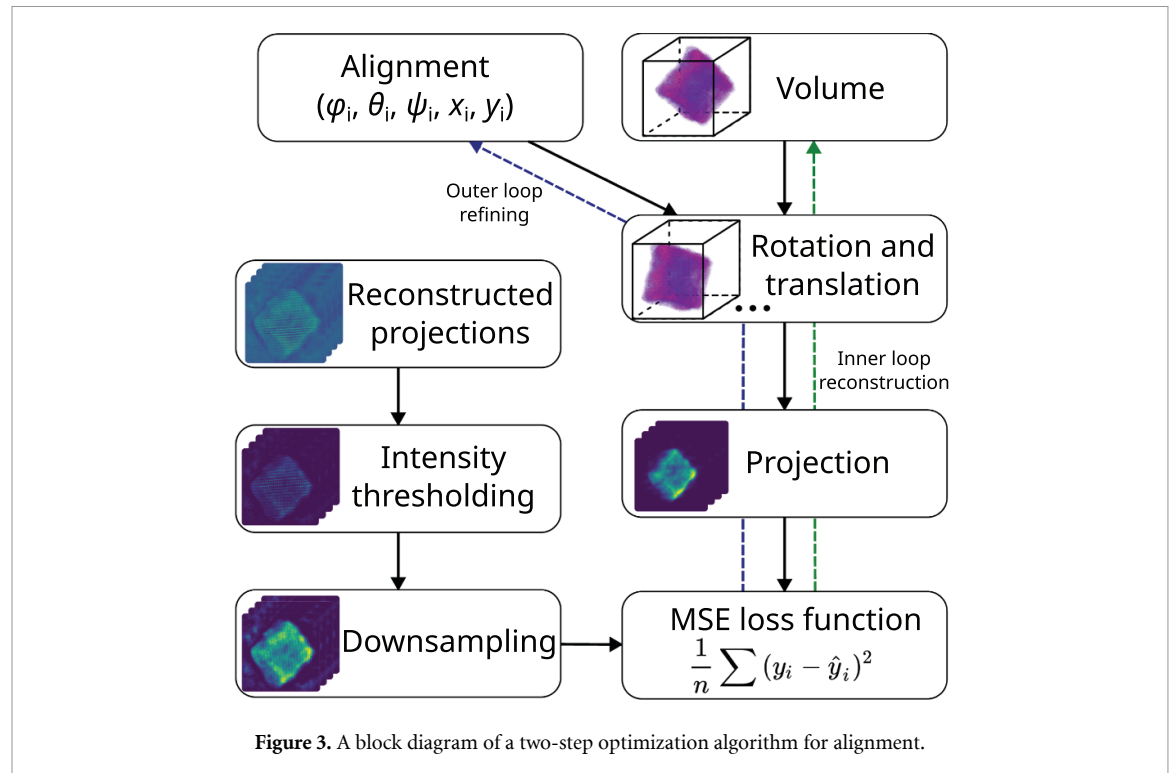


Figure 3. A block diagram of a two-step optimization algorithm for alignment.

accurately describes the outline of the nanocube. The projection images derived from this mask volume are then applied to the original ptychographic images to mask out substrate contrast outside of the nanocube. This approach compels a subsequent full-scale reconstruction to focus more intensively on the inner structure of the nanocube.

We conducted the final reconstruction at full resolution with additional implementation of Gaussian blurring with $\sigma = 0.5$ pixel of the reconstructed volume to avoid populating frequencies beyond Nyquist. Two different views of the resulting volume are displayed in figures 2(c) and (d), clearly showing the resolved lattice over the whole reconstructed volume. See supplementary video 1 for a movie with the reconstructed volume.

3. Discussion

Due to the strong contrast of the amorphous carbon substrate, the reconstructed volume exhibits higher noise than volumes of metal nanoparticles reconstructed previously using ADF-STEM tomography, where the substrate scattering produces only a weak background that is less prominent in the raw data and can be subtracted as a preprocessing step [65]. Since the volume displays slowly varying contrast for the Co atomic peaks, instead of tracing atomic peaks one by one as done in previous AET work, we register the experimental Co lattice with the crystallographic model of the spinel phase Co_3O_4 by first finding roughly the right rotation manually then launching a fitting procedure for the Bragg peak positions in Fourier space for experimental and simulated volume, and by optimizing both volumes in real space for translation coincidence comparing a small part of the original volumes. This gives us the positions of the expected atomic sites of Co and O atoms. Peak-by-peak atom-tracing algorithms, as previously reported [33], proved unstable due to the varying contrast across the volume, stemming from the amorphous carbon substrate. The results of our atom fitting procedure are shown in figure 4. For better visual clarity, we show a small 3D rendering of a unit-cell scale subvolume in figure 4(a), where the coincidence of fitted model atoms and reconstructed volume is visible. In figures 4(b) and (c) we then show larger subvolumes rotated to different zone axes of the Co_3O_4 crystal. In figures 4(a)–(c) The reconstructed volume is shown in orange, while Co atoms of the fitted atomic model are shown in blue. The insets to the bottom right show the crystallographic model of spinel phase Co_3O_4 viewed along the same orientation as the reconstructed volume. It can be seen that along the low-order [001] and [110] zone axes in figures 4(b) and (c), single Co atoms are easily distinguishable. However, there is inhomogeneous contrast across the subvolume stemming from the contribution of the substrate contrast.

Figures 4(d)–(f) contain slices through the larger subvolume with the simulated atomic potential as inset. The [100] direction in (d) is close to perpendicular to the missing wedge and has sufficient resolution to

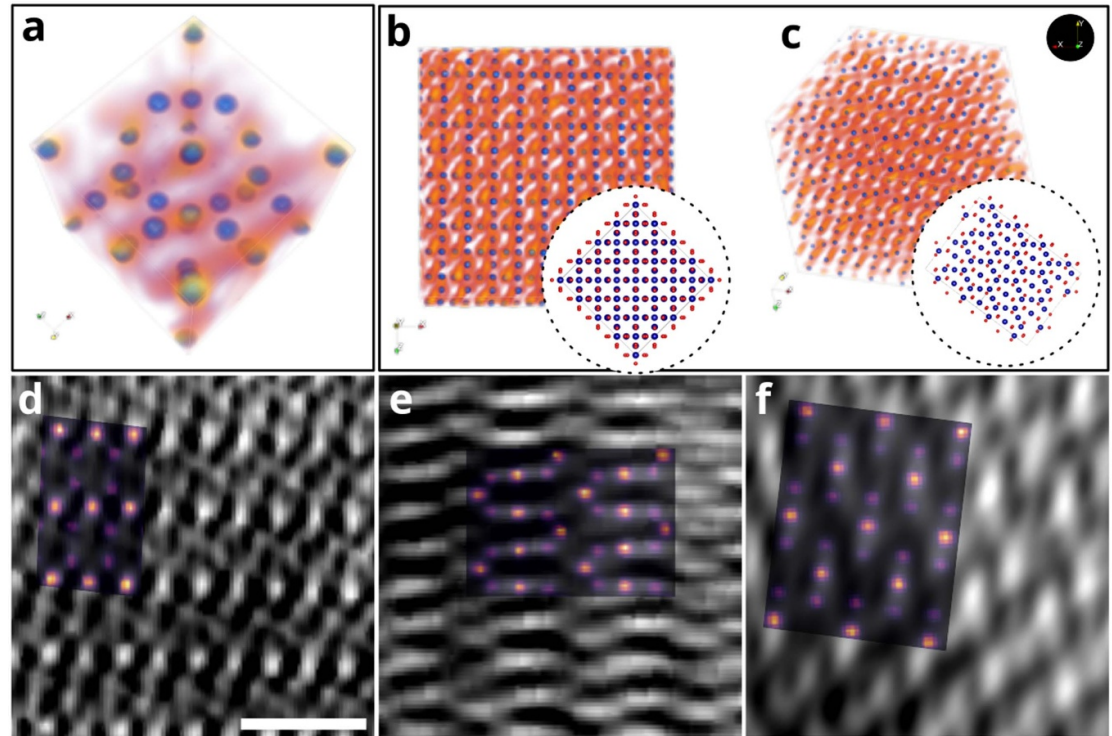


Figure 4. (a) Unit-cell scale subvolume of size $1 \times 1 \times 1 \text{ nm}^3$ showing the reconstruction in blue and the fitted model atoms in orange. (b), (c) Central subvolume of size $2.8 \times 2.8 \times 2.8 \text{ nm}^3$ viewed from different directions in orthographic projection. (b) [001], (c) [110]. Insets: atomic model of spinel phase Co_3O_4 viewed the corresponding direction. (d)–(f) slices through the larger subvolume along the (d) [100] (e) [010] (f) [001] directions. Inset: simulated atomic potential in this direction, with bright atoms as Co and weak atoms as O. Scale bar in (d)–(f): 1 nm.

resolve oxygen atoms. It can be seen that the background level in the reconstruction competes with the oxygen atom contrast. Along the other two directions in figures 4(e) and (f), the resolution is too low to distinguish Co and O atoms. We now turn to measuring the three-dimensional resolution using the 3D power spectrum.

To determine the resolution of the reconstruction, we analyzed the 3D spectral amplitude of the reconstructed volume. Figure 5 illustrates a spectral set of projections integrated over one or two axes. The resolution is estimated based on the last peak position for each projection, as shown in figure 5(a). For X and Z axes, it is 1.43 \AA^{-1} , corresponding to 0.7 \AA for d_{\perp_x} and d_{\perp_z} perpendicular to the missing wedge. For the Y axis, it is 0.49 \AA^{-1} , equivalent to 2.04 \AA for d_{\parallel} along the missing wedge. This is enough to resolve neighboring Co atoms, the minimal distance between which in the lattice is 2.8 \AA . Although the minimal distance between Co and O atoms of 1.558 \AA is comparable to the obtained resolution, our simulations of the electrostatic potential performed for two neighboring, isolated Co and O atoms showed that a point spread function of 1 \AA FWHM is required to successfully resolve the oxygen atoms in the lattice since the oxygen peaks are about 2.7 times weaker than Co peaks. We obtained this required resolution value as an FWHM of Gaussian blur applied to the simulated electrostatic potential to preserve a 26.3% dip between two peaks according to the Rayleigh criterion. It should be noted that the resolution of ptychographic reconstructions is element-specific [9]. Therefore, the required resolution to resolve weak scatterers next to strongly scattering atoms must be determined case-by-case.

To estimate an error of reconstruction, we also initiated a search for local maxima using the gradient descent method, employing the atomic positions obtained in the previous step as the starting points. This approach enabled us to identify various shifts in the lattice and missing Co atoms within the reconstructed volume, particularly where multiple initial positions converged to the same site. For the cubic structure, we discovered 30 401 Co atoms and identified 7656 missing sites, indicating that we successfully reconstructed 80% of the Co atoms. The mean displacement along perpendicular to the missing wedge directions (X, Z) is 0.5 \AA , while along the missing wedge direction (Y) it is 0.9 \AA , resulting in an overall mean displacement distance of 1.3 \AA . Although these values are smaller than our estimated resolution, they are still substantial enough to hinder precise lattice recovery. It's important to note that this approach assumes the actual nanocube lattice is free from line defects; otherwise, the number of displaced atoms would be significantly higher.

Finding point defects in the volume with the current data quality is therefore difficult.

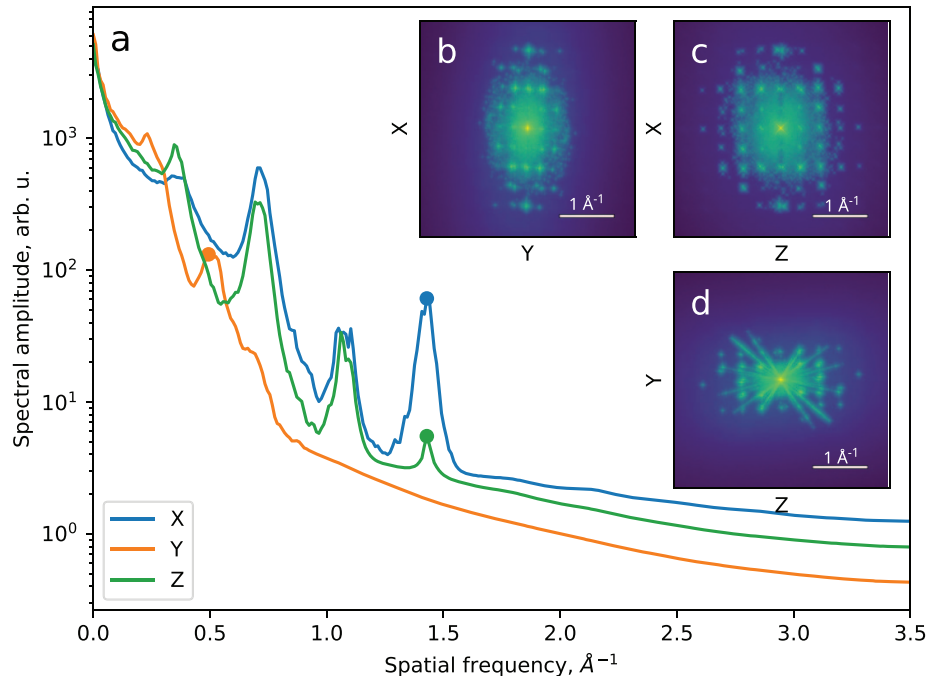


Figure 5. The spectral amplitude of the reconstructed volume, projected (via integration) onto axes X , Y , Z (a) and onto planes XY , XZ , YZ (b), (c), (d) respectively. Axes X and Z are perpendicular to the missing wedge, and Y aligns with the missing wedge direction. Points indicate the highest-resolution peak in the power spectrum. Scale bar in (b)–(d) 1 \AA^{-1} .

4. Conclusion

We have demonstrated 3D phase-contrast imaging using a sequential MSPT approach at an axial resolution of 2.04 \AA and transverse resolution of 0.7 \AA in a reconstructed volume of $(18.2 \text{ nm})^3$, surpassing the depth-of-field limit of 3D phase-contrast electron microscopy by a factor of 3.7, and the depth resolution record of MSP by a factor of 13.5. The relatively high number of missed atomic sites using an adapted atomic fitting procedure suggests that the sequential reconstruction alone may not be sufficient to resolve single light atoms in nanoparticles on amorphous substrate. The sequential reconstruction approach demonstrated here may serve as an input to a subsequent joint reconstruction in the future. The thickness limits of multi-slice ptychography are sample- and detector-dependent, but simulations suggest that reconstructing crystalline oxide samples with 70 nm thickness is feasible with currently available hardware [9]. This directly carries over to the thickness limits of MSPT, such that recovery of volumes containing more than one million atoms should be possible. Reaching such a scale will greatly expand the phenomena studied at 3D atomic resolution.

Due to the 2 \AA resolution in the missing wedge direction, the high background level inside the nanocube, and the low detection efficiency of the 4Dcamera prototype at 200 keV electron energy, we could not reliably resolve the oxygen atoms in the Co_3O_4 lattice in 3D. A further complication for MSPT of nanoparticles is the higher background level due to the amorphous substrate's strong contrast. This background cannot simply be subtracted as in ADF-STEM tomography [66]. Since the first demonstrations of ptychographic electron tomography reconstructed thin objects over vacuum [30, 31], and most published results on atomic resolution multi-slice ptychography study crystalline thin-films without substrate, this raises the question of whether crystalline substrates should be adopted for phase-contrast tomography of weakly scattering atoms at atomic resolution until the method has progressed to the point where weakly scattering amorphous materials can be resolved atom-by-atom. We think there is enough room for improvement in algorithmic aspects, experimental design, and hardware by increasing the detection efficiency of the fast-framing 4D-STEM detector such that this point can be reached soon.

Compared to a joint ptychography-tomography reconstruction algorithm [58], the sequential approach presented here allows the disentangling of the alignment procedure and precise estimation of Euler angles and translation from the tomographic reconstruction. From a practical point of view, the question of how all parameters of such a joint reconstruction can be initialized with a sufficiently good initial guess is still unsolved. Our sequential MSPT approach, which yields initial estimates for all tilt-dependent probes, subpixel probe positions, and initial Euler angles, may be used to bootstrap such a joint reconstruction [67].

A promising avenue is using more explicit atomistic models in ptychographic tomography, as recently demonstrated in multi-slice ptychography. Directly modeling atoms in the forward pass allows us to more accurately describe thermal diffuse scattering [68] and improve the resolution of multi-slice ptychography further [69]. Certainly, ptychographic electron tomography has an advantage over the ADF-STEM-based method in terms of experimental automation since precise focusing is not required for electron ptychography. This results in less challenging, although more data-intensive experiments, and indicates a bright future for large-scale, high-resolution 4D-STEM-based three-dimensional imaging.

Data availability statement

The data that support the findings of this study are openly available at the following URL/DOI: <https://doi.org/10.5281/zenodo.13836702>.

Code availability statement

The code is available on Github under the following link: https://github.com/ECLIPSE-Lab/MSPT_code.

Acknowledgments

P P is supported by the Strobe STC research center, Grant No. DMR 1548924 and by an EAM starting grant project ScatterEM. M C S is supported by the Strobe STC research center, Grant No. DMR 1548924. A R is supported by an EAM Starting grant project, ScatterEM. M G C. is funded by the U.S. Department of Energy in the program 4D Camera Distillery: From Massive Electron Microscopy Scattering Data to Useful Information with AI/ML. Work at the Molecular Foundry was supported by the Office of Science, Office of Basic Energy Sciences, of the U.S. Department of Energy under Contract No. DE-AC02-05CH11231. P P gratefully acknowledges the scientific support and HPC resources provided by the Erlangen National High Performance Computing Center (NHR@FAU) of the Friedrich-Alexander-Universität Erlangen-Nürnberg (FAU) under the NHR project AtomicTomo3D. NHR funding is provided by federal and Bavarian state authorities. NHR@FAU hardware is partially funded by the German Research Foundation (DFG)—440719683. The 4D Camera was developed under the DOE BES Accelerator and Detector Research Program in collaboration with Gatan, Inc. We thank Peter Ercius for their help with 4Dcamera data acquisition and Colin Ophus for helpful discussions. We want to thank Gatan, Inc. as well as P Denes, A Minor, J Ciston, J Joseph, and I Johnson, who contributed to the development of the 4D Camera.

Author contributions

A R: Methodology, Investigation, Writing—original draft, Visualization.

M C S: Investigation, Writing—Review & Editing, Funding acquisition.

M C: Investigation, Writing—Review & Editing.

P M P: Conceptualization, Investigation, Writing—original draft, Writing—Review & Editing, Funding acquisition, Project administration.

ORCID iDs

Andrey Romanov  <https://orcid.org/0000-0001-6342-6568>

Min Gee Cho  <https://orcid.org/0000-0003-4490-7352>

Mary Cooper Scott  <https://orcid.org/0000-0002-9543-6725>

Philipp Pelz  <https://orcid.org/0000-0002-8009-4515>

References

- [1] Lazić I, Bosch E G T and Lazar S 2016 Phase contrast STEM for thin samples: integrated differential phase contrast *Ultramicroscopy* **160** 265–80
- [2] Ooe K, Seki T, Yoshida K, Kohno Y, Ikuhara Y and Shibata N 2023 Direct imaging of local atomic structures in zeolite using optimum bright-field scanning transmission electron microscopy *Sci. Adv.* **9** eadf6865
- [3] Yang H *et al* 2016 Simultaneous atomic-resolution electron ptychography and Z-contrast imaging of light and heavy elements in complex nanostructures *Nat. Commun.* **7** 12532
- [4] Peng X *et al* 2022 Observation of formation and local structures of metal-organic layers via complementary electron microscopy techniques *Nat. Commun.* **13** 5197
- [5] Sha H, Cui J, Li J, Zhang Y, Yang W, Li Y and Yu R 2023 Ptychographic measurements of varying size and shape along zeolite channels *Sci. Adv.* **9** eadfl151

- [6] Lozano J G, Martinez G T, Jin L, Nellist P D and Bruce P G 2018 Low-dose aberration-free imaging of Li-rich cathode materials at various states of charge using electron ptychography *Nano Lett.* **18** 6850–5
- [7] dos Reis R, Yang H, Ophus C, Ercius P, Bizarri G, Perrodin D, Shalapska T, Bourret E, Ciston J and Dahmen U 2018 Determination of the structural phase and octahedral rotation angle in halide perovskites *Appl. Phys. Lett.* **112** 071901
- [8] Gao S, Wang P, Zhang F, Martinez G T, Nellist P D, Pan X and Kirkland A I 2017 Electron ptychographic microscopy for three-dimensional imaging *Nat. Commun.* **8** 163
- [9] Chen Z, Jiang Y, Shao Y-T, Holtz M E, Odstrčil M, Guizar-Sicairos M, Hanke I, Ganschow S, Schlom D G and Muller D A 2021 Electron ptychography achieves atomic-resolution limits set by lattice vibrations *Science* **372** 826–31
- [10] O’Leary C M, Zhang J, Su C, Kahn S, Jiang H, Zettl A, Ciston J and Miao J 2023 Three-dimensional imaging of buried interfaces with multislice ptychography (arXiv:2308.15471)
- [11] Zhang H *et al* 2023 Three-dimensional inhomogeneity of zeolite structure and composition revealed by electron ptychography *Science* **380** 633–8
- [12] Sha H, Ma Y, Cao G, Cui J, Yang W, Li Q and Yu R 2023 Sub-nanometer-scale mapping of crystal orientation and depth-dependent structure of dislocation cores in SrTiO₃ *Nat. Commun.* **14** 162
- [13] Sha H, Cui J and Yu R 2022 Deep sub-angstrom resolution imaging by electron ptychography with misorientation correction *Sci. Adv.* **8** eabn2275
- [14] Chen Z, Shao Y-T, Jiang Y and Muller D 2021 Three-dimensional imaging of single dopants inside crystals using multislice electron ptychography *Microsc. Microanal.* **27** 2146–8
- [15] Xin H L and Muller D A 2009 Aberration-corrected ADF-STEM depth sectioning and prospects for reliable 3D imaging in S/TEM *J. Electron Microsc.* **58** 157–65
- [16] Behan G, Cosgriff E C, Angus I K and Peter D N 2009 Three-dimensional imaging by optical sectioning in the aberration-corrected scanning transmission electron microscope *Phil. Trans. R. Soc. A* **367** 3825–44
- [17] Van den Broek W, Van Aert S and Van Dyck D 2010 A model based reconstruction technique for depth sectioning with scanning transmission electron microscopy *Ultramicroscopy* **110** 548–54
- [18] Ishikawa R, Lupini A R, Findlay S D, Taniguchi T and Pennycook S J 2014 Three-dimensional location of a single dopant with atomic precision by aberration-corrected scanning transmission electron microscopy *Nano Lett.* **14** 1903–8
- [19] Ishikawa R, Lupini A R, Hinuma Y and Pennycook S J 2015 Large-angle illumination STEM: toward three-dimensional atom-by-atom imaging *Ultramicroscopy* **151** 122–9
- [20] Ishikawa R, Shibata N, Taniguchi T and Ikuhara Y 2020 Three-dimensional imaging of a single dopant in a crystal *Phys. Rev. Appl.* **13** 034064
- [21] Yang H, Lozano J G, Pennycook T J, Jones L, Hirsch P B and Nellist P D 2015 Imaging screw dislocations at atomic resolution by aberration-corrected electron optical sectioning *Nat. Commun.* **6** 7266
- [22] Hovden R, Xin H L and Muller D A 2011 Extended depth of field for high-resolution scanning transmission electron microscopy *Microsc. Microanal.* **17** 75–80
- [23] Robert H L, Lobato I, Lyu F J, Chen Q, Van Aert S, Van Dyck D and Müller-Caspary K 2022 Dynamical diffraction of high-energy electrons investigated by focal series momentum-resolved scanning transmission electron microscopy at atomic resolution *Ultramicroscopy* **233** 113425
- [24] Brown H G *et al* 2022 A three-dimensional reconstruction algorithm for scanning transmission electron microscopy data from a single sample orientation *Microsc. Microanal.* **28** 1632–40
- [25] Terzoudis-Lumsden E W C, Petersen T C, Brown H G, Pelz P M, Ophus C and Findlay S D 2023 Resolution of virtual depth sectioning from four-dimensional scanning transmission electron microscopy *Microsc. Microanal.* **29** 1409–21
- [26] Rose H 2022 Minimum-dose phase-contrast tomography by successive numerical optical sectioning employing the aberration-corrected stem and a pixelated detector *Ultramicroscopy* **235** 113484
- [27] Lee Z, Kaiser U and Rose H 2019 Prospects of annular differential phase contrast applied for optical sectioning in stem *Ultramicroscopy* **196** 58–66
- [28] Bosch E G T and Lazić I 2019 Analysis of depth-sectioning stem for thick samples and 3D imaging *Ultramicroscopy* **207** 112831
- [29] Ding Z *et al* 2022 Three-dimensional electron ptychography of organic–inorganic hybrid nanostructures *Nat. Commun.* **13** 4787
- [30] Hofer C, Mustonen K, Skakalova V and Pennycook T J 2023 Picometer-precision few-tilt ptychotomography of 2D materials *2D Mater.* **10** 035029
- [31] Pelz P M, Griffin S M, Stonemeyer S, Popple D, DeVylde H, Ercius P, Zettl A, Scott M C and Ophus C 2023 Solving complex nanostructures with ptychographic atomic electron tomography *Nat. Commun.* **14** 7906
- [32] Scott M C, Chen C-C, Mecklenburg M, Zhu C, Xu R, Ercius P, Dahmen U, Regan B C and Miao J 2012 Electron tomography at 2.4-ångström resolution *Nature* **483** 444–7
- [33] Miao J, Ercius P and Billinge S J L 2016 Atomic electron tomography: 3D structures without crystals *Science* **353** eaaf2157
- [34] Hovden R, Ercius P, Jiang Y, Wang D, Yu Y, Abruna H D, Elser V and Muller D A 2014 Breaking the crowther limit: Combining depth-sectioning and tilt tomography for high-resolution, wide-field 3D reconstructions *Ultramicroscopy* **140** 26–31
- [35] Hovden R 2014 Atomic imaging with highly convergent electron beams (available at: <https://ecommons.cornell.edu/handle/1813/36158>)
- [36] Dahmen T 2015 Tomographic reconstruction of combined tilt- and focal series in scanning transmission electron microscopy *PhD Thesis* Universität des Saarlandes (<https://doi.org/10.22028/D291-26625>)
- [37] Dahmen T, Baudoin J-P, Lupini A R, Kübel C, Slusallek P and de Jonge N 2014 Combined scanning transmission electron microscopy tilt- and focal series *Microsc. Microanal.* **20** 548–60
- [38] Dahmen T, Kohr H, de Jonge N and Slusallek P 2015 Matched backprojection operator for combined scanning transmission electron microscopy tilt- and focal series *Microsc. Microanal.* **21** 725–38
- [39] Yalisove R, Hyun Sung S, Ercius P and Hovden R 2021 Limits of three-dimensional resolution and dose for aberration-corrected electron tomography *Phys. Rev. Appl.* **15** 014003
- [40] Maiden A M, Humphry M J and Rodenburg J M 2012 Ptychographic transmission microscopy in three dimensions using a multi-slice approach *J. Opt. Soc. Am. A* **29** 1606–14
- [41] Tsai E H R, Usov I, Diaz A, Menzel A and Guizar-Sicairos M 2016 X-ray ptychography with extended depth of field *Opt. Express* **24** 29089–108
- [42] Hu J, Li S, Xie H and Shen Y 2022 Multi-slice ptychographic imaging with multistage coarse-to-fine reconstruction *Opt. Express* **30** 21211–29

- [43] Dierolf M, Menzel A, Thibault P, Schneider P, Kewish C M, Wepf R, Bunk O and Pfeiffer F 2010 Ptychographic x-ray computed tomography at the nanoscale *Nature* **467** 436–9
- [44] Chang H, Enfedaque P and Marchesini S 2019 Iterative joint ptychography-tomography with total variation regularization 2019 *IEEE Int. Conf. on Image Processing (ICIP)* (IEEE) pp 2931–5
- [45] Kahnt M, Becher J, Brückner D, Fam Y, Sheppard T, Weissenberger T, Wittwer F, Grunwaldt J-D, Schwieger W and Schroer C G 2019 Coupled ptychography and tomography algorithm improves reconstruction of experimental data *Optica* **6** 1282–9
- [46] Aslan S, Nikitin V, Ching D J, Bicer T, Leyffer S and Gürsoy D 2019 Joint ptycho-tomography reconstruction through alternating direction method of multipliers *Opt. Express* **27** 9128–43
- [47] Nikitin V, Aslan S, Yao Y, Biçer T, Leyffer S, Mokso R and Gürsoy D 2019 Photon-limited ptychography of 3D objects via Bayesian reconstruction *OSA Contin.* **2** 2948–68
- [48] Li P and Maiden A 2018 Multi-slice ptychographic tomography *Sci. Rep.* **8** 2049
- [49] Kahnt M, Grote L, Brückner D, Seyrich M, Wittwer F, Koziej D and Schroer C G 2021 Multi-slice ptychography enables high-resolution measurements in extended chemical reactors *Sci. Rep.* **11** 1500
- [50] Gilles M A, Nashed Y S G, Du M, Jacobsen C and Wild S M 2018 3D x-ray imaging of continuous objects beyond the depth of focus limit *Optica* **5** 1078–86
- [51] Öztürk H, Yan H, He Y, Ge M, Dong Z, Lin M, Nazaretski E, Robinson I K, Chu Y S and Huang X 2018 Multi-slice ptychography with large numerical aperture multilayer Laue lenses *Optica* **5** 601–7
- [52] Jacobsen C 2018 Relaxation of the Crowther criterion in multislice tomography *Opt. Lett.* **43** 4811–4
- [53] Huang X et al 2019 Resolving 500 nm axial separation by multi-slice x-ray ptychography *Acta Crystallogr. A* **75** 336–41
- [54] Du M, Nashed Y S G, Kandel S, Gürsoy D and Jacobsen C 2020 Three dimensions, two microscopes, one code: automatic differentiation for x-ray nanotomography beyond the depth of focus limit *Sci. Adv.* **6** eaay3700
- [55] Shimomura K, Hirose M and Takahashi Y 2018 Multislice imaging of integrated circuits by precession x-ray ptychography *Acta Crystallogr. A* **74** 66–70
- [56] Van den Broek W and Koch C T 2013 General framework for quantitative three-dimensional reconstruction from arbitrary detection geometries in tem *Phys. Rev. B* **87** 184108
- [57] Chang D J, Kim D S, Rana A, Tian X, Zhou J, Ercius P and Miao J 2020 Ptychographic atomic electron tomography: towards three-dimensional imaging of individual light atoms in materials *Phys. Rev. B* **102** 174101
- [58] Lee J, Lee M, Park Y, Ophus C and Yang Y 2023 Multislice electron tomography using four-dimensional scanning transmission electron microscopy *Phys. Rev. Appl.* **19** 054062
- [59] Pei X et al 2023 Cryogenic electron ptychographic single particle analysis with wide bandwidth information transfer *Nat. Commun.* **14** 3027
- [60] Dabov K, Foi A, Katkovnik V and Egiazarian K 2007 Image denoising by sparse 3-D transform-domain collaborative filtering *IEEE Trans. Image Process.* **16** 2080–95
- [61] Oh M H et al 2020 Design and synthesis of multigrain nanocrystals via geometric misfit strain *Nature* **577** 359–63
- [62] Ophus C 2019 Four-dimensional scanning transmission electron microscopy (4D-STEM): from scanning nanodiffraction to ptychography and beyond *Microsc. Microanal.* **25** 563–82
- [63] Chen C-C, Zhu C, White E R, Chiu C-Y, Scott M C, Regan B C, Marks L D, Huang Y and Miao J 2013 Three-dimensional imaging of dislocations in a nanoparticle at atomic resolution *Nature* **496** 74–77
- [64] Paszke A et al 2019 PyTorch: an imperative style, high-performance deep learning library *Advances in Neural Information Processing Systems* vol 32
- [65] Yang Y et al 2017 Deciphering chemical order/disorder and material properties at the single-atom level *Nature* **542** 75–79
- [66] Yang Y et al 2021 Determining the three-dimensional atomic structure of an amorphous solid *Nature* **592** 60–64
- [67] You S, Romanov A and Pelz P 2024 Near-isotropic sub-Ångstrom 3D resolution phase contrast imaging achieved by end-to-end ptychographic electron tomography *Phys. Scr.* (<https://doi.org/10.1088/1402-4896/ad9a1a>)
- [68] Diederichs B, Herdegen Z, Strauch A, Filbir F and Müller-Caspary K 2024 Exact inversion of partially coherent dynamical electron scattering for picometric structure retrieval *Nat. Commun.* **15** 101
- [69] Yang W, Sha H, Cui J, Mao L and Yu R 2024 Local-orbital ptychography for ultrahigh-resolution imaging *Nat. Nanotechnol.* **19** 612–7